An exact Laplace transform formulation for a point source above a ground surface

Xiao Di and Kenneth E. Gilbert[a)]
National Center for Physical Acoustics, University, Mississippi 38677

(Received 16 December 1991; revised 10 September 1992; accepted 5 October 1992)

An exact analysis is given for a point source in air above a ground surface. By representing the plane-wave reflection coefficient as the Laplace transform of an image source distribution, a well-behaved image integral, instead of the usual Sommerfeld integral, is obtained. The approach is valid for both locally and extended reacting surfaces. For a locally reacting ground surface, the image integral is an especially simple, rapidly convergent integral. The integral for local reaction is investigated analytically for a number of limiting cases. The resulting analytic solutions are compared with analytic solutions obtained from more standard approaches. Finally, the image integral for local reaction is analyzed numerically, and an upper limit on the numerical integration is given. It is shown that with realistic values of ground impedance, the prescribed integration limit allows the image integral to be easily and accurately computed numerically.

PACS numbers: 43.28.Fp, 43.20.Fn

INTRODUCTION

The sound field resulting from a point source above the ground has been studied by many authors.[1-12] For a homogeneous atmosphere, the problem is the so-called Sommerfeld problem, which has a solution involving a difficult Sommerfeld integral. To evaluate the Sommerfeld integral, various assumptions and approximations have been adopted.[1-12] In contrast, we use an exact method based on an image source distribution. The method was originally proposed by Lindell and Alanen for vertical electric and magnetic dipoles in radiowave propagation.[13,14] With the image formulation, the reflection coefficient is expressed as a Laplace transform over an image source function. The final expression for the acoustic field involves a well-behaved image integral instead of the usual Sommerfeld integral.

The reflection coefficient for an extended reacting surface has essentially the same form as the reflection coefficient for an electric dipole. Consequently, the derivation for extended reaction is very similar to that given in Ref. 14. For a locally reacting surface, however, the reflection coefficient has a different form from that of either an electric or magnetic dipole.[13,14] Nevertheless, the image method is still applicable, and, in fact, is much simpler to apply than for an extended reacting surface. For a locally reacting surface, the image source contribution can be easily obtained from a very simple image source integral. The integrand is well-behaved, and the integral converges rapidly for a realistic ground impedance. Because the integral is well behaved and convergent, it is straightforward to develop criteria for accurate numerical evaluation of the integral.

I. IMAGE THEORY

Consider a point source located at a height h above the ground with the coordinates $(x, y, z) = (0, 0, h)$, as shown in Fig. 1. Here ρ_1 and k_1 are, respectively, the density and wave number for air. The corresponding effective quantities for air within porous ground are taken to be ρ_2 and k_2. To account for viscous and thermal dissipation of sound in the ground, we take ρ_2 and k_2 to be complex.

The complex pressure field for a constant frequency point source at $(0, 0, h)$ satisfies the following equations:

$$(\nabla^2 + k_1^2)P_1 = -4\pi\delta(\bar{r} - \hat{z}h), \quad z > 0, \tag{1}$$

$$(\nabla^2 + k_2^2)P_2 = 0, \quad z < 0, \tag{2}$$

where P_1 and P_2 are sound pressures in the air $(z<0)$ and in the porous ground $(z<0)$, respectively. The observation

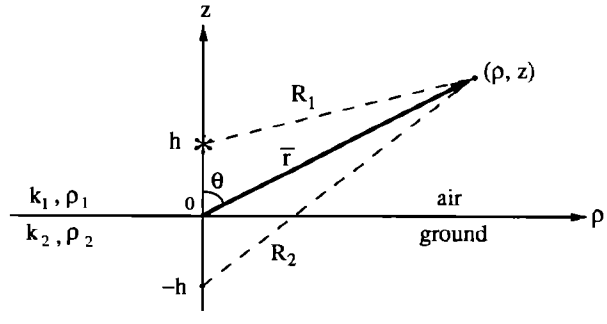

FIG. 1. A point source above a ground plane. The point source is located at $(x,y,z) = (0,0,h)$. The wave number and density for the air are ρ_1 and k_1, respectively. The corresponding effective quantities for air within the porous ground are ρ_2 and k_2. The receiver is located at $r = (\rho,z)$, where $\rho = (x^2 + y^2)^{1/2}$. The variables R_1 and R_2 are the distance between source and receiver and image source and receiver, respectively.

[a)] Present address: Applied Research Laboratory and the Graduate Program in Acoustics, Pennsylvania State University, P.O. Box 30, State College, PA 16804.

 0001-4966/93/020714-07$06.00

point is $\bar{r}$ and $\hat{z}$ is a vertical unit vector. The boundary conditions at the air–ground interface are

$$P_1 = P_2, \quad z = 0. \tag{3}$$

$$\frac{1}{\rho_1}\frac{\partial P_1}{\partial z} = \frac{1}{\rho_2}\frac{\partial P_2}{\partial z}, \quad z = 0. \tag{4}$$

Fourier transforming Eqs. (1)–(4) with respect to the horizontal plane (x and y), gives

$$\frac{\partial^2 \tilde{P}_1}{\partial z^2} + k_{1z}^2 \tilde{P}_1 = -4\pi\delta(z-h), \quad z>0, \tag{5}$$

$$\frac{\partial^2 \tilde{P}_2}{\partial z^2} + k_{2z}^2 \tilde{P}_2 = 0, \quad z<0, \tag{6}$$

$$\tilde{P}_1 = \tilde{P}_2, \quad z = 0, \tag{7}$$

$$\frac{1}{\rho_1}\frac{\partial \tilde{P}_1}{\partial z} = \frac{1}{\rho_2}\frac{\partial \tilde{P}_2}{\partial z}, \quad z = 0, \tag{8}$$

where

$$k_{1z} = \sqrt{k_1^2 - k_x^2 - k_y^2} \tag{9}$$

and

$$k_{2z} = \sqrt{k_2^2 - k_x^2 - k_y^2} = \sqrt{(k_2^2 - k_1^2) + k_{1z}^2} \tag{10}$$

are the vertical wave numbers for $z>0$ and $z<0$, respectively. The solution in the k_x, k_y, and z domain is

$$\tilde{P}_1 = A\{\exp(ik_{1z}|z-h|) + R(k_{1z}) \times \exp[ik_{1z}(z+h)]\}, \quad z>0, \tag{11}$$

$$\tilde{P}_2 = A(1+R(k_{1z}))\exp(ik_{1z}h) \times \exp(-ik_{2z}z), \quad z<0, \tag{12}$$

with

$$A = 2\pi i/k_{1z} \tag{13}$$

and

$$R(k_{1z}) = \frac{\rho_2 k_{1z} - \rho_1 k_{2z}}{\rho_2 k_{1z} + \rho_1 k_{2z}} = \frac{\rho_2 k_{1z} - \rho_1\sqrt{(k_2^2 - k_1^2) + k_{1z}^2}}{\rho_2 k_{1z} + \rho_1\sqrt{(k_2^2 - k_1^2) + k_{1z}^2}}, \tag{14}$$

where $R(k_{1z})$ is the plane-wave reflection coefficient.

Equation (11) suggests that the solution above the ground can be separated into two parts: the direct free-space wave from the physical source at (0, 0, h) and a reflected wave from an image source. The strength and location of the image source is to be determined. With this decomposition in mind, we write the total field as the sum of a free-space component and an image component,

$$\tilde{P}_1 = \tilde{P}_{\text{free}} + \tilde{P}_{\text{image}}, \quad z>0, \tag{15}$$

where

$$\tilde{P}_{\text{free}} = A\exp(ik_{1z}|z-h|), \tag{16}$$

$$\tilde{P}_{\text{image}} = AR(k_{1z})\exp[ik_{1z}(z+h)]. \tag{17}$$

At this point, inverse Fourier transforming $\tilde{P}_1$ in Eq. (11) with respect to k_x and k_y would lead to the standard Sommerfeld result. An alternative approach, based on Refs. 13 and 14, is to assume that the reflection coefficient $R(k_{1z})$ can be represented by a Laplace transform,

$$R(k_{1z}) = \int_0^\infty s(q)e^{-q(\epsilon k_{1z})}\,dq, \tag{18}$$

where $s(q)$ is an image source distribution that will be determined later. The factor ϵ multiplying k_{1z} in the exponential is left arbitrary for the moment so that we can later apply Eq. (18) to both extended and locally reacting surfaces. As will be shown in the next section, we used $\epsilon = 1$ and $\epsilon = (k_2^2 - k_1^2)^{-1/2}$, respectively, to obtain $s(q)$ for locally reacting and extended reacting surfaces.

Upon substituting Eq. (18) into Eq. (17), we obtain

$$\tilde{P}_{\text{image}} = \int_0^\infty s(q)\{Ae^{ik_{1z}[z+(h+i\epsilon q)]}\}dq. \tag{19}$$

Now we substitute Eqs. (19) and (16) into Eq. (15) and perform the inverse Fourier transform with respect to k_x and k_y. Note that part inside the { } in Eq. (19) has the same form as the free-space expression given in Eq. (16). Since the free-space result is a known analytic expression we can write immediately,

$$P_{\text{free}}(\bar{r}) = \frac{e^{ik_1|\bar{r}-\hat{z}h|}}{|\bar{r}-\hat{z}h|} \tag{20}$$

and

$$P_{\text{image}}(\bar{r}) = \int_0^\infty s(q)\frac{e^{ik_1|\bar{r}+\hat{z}(h+i\epsilon q)}}{|\bar{r}+\hat{z}(h+i\epsilon q)|}\,dq, \tag{21}$$

with

$$|\bar{r}+\hat{z}(h+i\epsilon q)| \equiv \sqrt{\rho^2 + (z+h+i\epsilon q)^2}, \tag{22}$$

where the root is in the first quadrant and $\rho = \sqrt{x^2+y^2}$ is the horizontal distance. To obtain Eq. (21), the order of the Fourier transform and the Laplace transform were interchanged so that we obtain the integral of a source distribution times a free-space Green's function with a complex source position. Combining Eq. (20) and Eq. (21), gives

$$P_1(\bar{r}) = \frac{e^{ik_1|\bar{r}-\hat{z}h|}}{|\bar{r}-\hat{z}h|} + \int_0^\infty s(q)\frac{e^{ik_1|\bar{r}+\hat{z}(h+i\epsilon q)|}}{|\bar{r}+\hat{z}(h+i\epsilon q)|}\,dq. \tag{23}$$

In Eq. (23), the total field above the ground has been expressed as a sum of the original point source field and the field from an image line source distribution $s(q)$ in a homogeneous complex space, with the image located at (0, 0, $-h-i\epsilon q$).

II. IMAGE SOURCE DISTRIBUTION

The exact image source distribution $s(q)$, which has been defined in Eq. (18), is obtained from the inverse Laplace transform. Although we are primarily interested in the result for a locally reacting surface, for the sake of completeness we first outline the form of the solution for the extended reaction.

A. Extended reacting surface

The reflection coefficient $R(k_{1z})$ in Eq. (14) can be written as

$$R(k_{1z}) = \frac{\rho_2 k_{1z} - \rho_1\sqrt{(k_2^2 - k_1^2) + k_{1z}^2}}{\rho_2 k_{1z} + \rho_1\sqrt{(k_2^2 - k_1^2) + k_{1z}^2}}$$
$$= \frac{\rho_2(\epsilon k_{1z}) - \rho_1\sqrt{(\epsilon k_{1z})^2 + 1}}{\rho_2(\epsilon k_{1z}) + \rho_1\sqrt{(\epsilon k_{1z})^2 + 1}}$$
$$= \frac{\rho_2 - \rho_1}{\rho_2 + \rho_1} - \frac{\rho_2 - \rho_1}{\rho_2 + \rho_1}\frac{\rho_2}{\rho_1}\frac{\gamma^2}{(\epsilon k_{1z})^2 - \gamma^2}$$
$$+ \frac{\rho_2}{\rho_1}\frac{\gamma^2}{(\epsilon k_{1z})^2 - \gamma^2}\left[(\epsilon k_{1z}) - \sqrt{(\epsilon k_{1z})^2 + 1}\right], \tag{24}$$

where $\epsilon = 1/\sqrt{k_2^2 - k_1^2}$ and $\gamma = \rho_1/\sqrt{\rho_2^2 - \rho_1^2}$.

As indicated in Eq. (18), we can obtain the image source distribution $s(q)$ by using an inverse Laplace transform. With the expression in Eq. (24) for $R(k_{1z})$ the result for $s(q)$ is

$$s(q) = \frac{\rho_2 - \rho_1}{\rho_2 + \rho_1}\delta(q) - \gamma\frac{\rho_2}{\rho_1}\frac{\rho_2 - \rho_1}{\rho_2 + \rho_1}\sinh(\gamma q)$$
$$+ 2\gamma\frac{\rho_2}{\rho_1}\int_0^q \sinh[\gamma(q - q')]\frac{J_2(q')}{q'}dq'$$
$$= \frac{\rho_2 - \rho_1}{\rho_2 + \rho_1}\delta(q) - \gamma\frac{\rho_2}{\rho_1}\int_0^\infty e^{-\gamma q'}$$
$$\times\left(\frac{J_2(q' + q)}{q' + q} - \frac{J_2(q' - q)}{q' - q}\right)dq'. \tag{25}$$

Using the above image strength $s(q)$ in Eq. (23), gives the total sound pressure above a surface with extended reaction. Since the image strength itself involves an integral, the necessary calculation is a double integration. However, the numerical calculation can be easily done. The procedure is similar to that given in Ref. 14 for electromagnetic waves.

B. Locally reacting surface

For many naturally occurring ground surfaces, the local reaction approximation is valid. For such surfaces the Laplace transform representation of the reflection coefficient simplifies considerably since we have $k_{2z} \approx k_2$, and

$$R(k_{1z}) = \frac{\rho_2 k_{1z} - \rho_1 k_{2z}}{\rho_2 k_{1z} + \rho_1 k_{2z}} \approx \frac{\rho_2 k_{1z} - \rho_1 k_2}{\rho_2 k_{1z} + \rho_1 k_2}$$
$$= \frac{k_{1z} - k_1/Z_g}{k_{1z} + k_1/Z_g}, \tag{26}$$

where $Z_g = R + iX$ is the normalized specific acoustic ground impedance. The image source distribution $s(q)$ obtained by computing the inverse Laplace transform of $R(k_{1z})$ is

$$s(q) = \delta(q) - 2(k_1/Z_g)e^{-(k_1/Z_g)q}, \tag{27}$$

where for local reaction, ϵ in Eq. (18) is taken to be 1. Use of the above result for the image strength $s(q)$ in Eq. (23) gives

$$P_1(\bar{r}) = \frac{e^{ik_1|\bar{r} - \hat{z}h|}}{|\bar{r} - \hat{z}h|} + \frac{e^{ik_1|\bar{r} + \hat{z}h|}}{|\bar{r} + \hat{z}h|}$$
$$- 2\frac{k_1}{Z_g}\int_0^\infty e^{-(k_1/Z_g)}\frac{e^{ik_1|\bar{r} + \hat{z}(h + iq)|}}{|\bar{r} + \hat{z}(h + iq)|}dq \tag{28}$$

or

$$P_1(\bar{r}) = \frac{e^{ik_1R_1}}{R_1} + \frac{e^{ik_1R_2}}{R_2} - 2\frac{k_1}{Z_g}\int_0^\infty e^{-(k_1/Z_g)q}$$
$$\times\frac{e^{ik_1|\bar{r} + \hat{z}(h + iq)|}}{|\bar{r} + \hat{z}(h + iq)|}dq, \tag{29}$$

where $R_1 = |\bar{r} - \hat{z}h|$ and $R_2 = |\bar{r} + \hat{z}h|$.

Equation (29) shows that the image source contribution to the sound field above the ground comes from a mirror-image point source (the second term) plus an image integral. Since k_1 is real and positive, and Z_g is a complex number with a positive real part, most of the contribution to the integral in Eq. (29) comes from moderate values of q. As will be discussed in Sec. IV, the numerical evaluation of the integral in Eq. (29) is straightforward. The ease with which Eq. (29) can be numerically computed is one of the main points of this article. [Note that the sign of $\exp(ik_1/R_2)/R_2$ in Eq. (29), is necessarily positive in our Laplace transform formulation but in the Sommerfeld formulation may be chosen to be either positive or negative.]

III. LIMITING CASES

Before discussing the numerical evaluation of the integral in Eq. (29) it is worthwhile to first consider some limiting cases that can be given analytically.

For $Z_g = \infty$ and $Z_g = 0$, Eq. (29) becomes the expected source and perfect image

$$P_1(\bar{r}) = \frac{e^{ik_1R_1}}{R_1} \pm \frac{e^{ik_1R_2}}{R_2}, \tag{30}$$

where the (+) and (−) are for $Z_g = \infty$ and $Z_g = 0$, respectively.

When the source and receiver are on the same vertical line ($|\bar{r}| = z$), and $z + h \gg \lambda$ [$|Z_g|/\text{real}(Z_g)$], where λ is the wavelength in air, Eq. (29) gives

$$P_1(\bar{r}) = \frac{e^{ik_1R_1}}{R_1} + \frac{e^{ik_1R_2}}{R_2} - 2\frac{k_1}{Z_g}\int_0^\infty e^{-(k_1/Z_g)q}$$
$$\times\frac{e^{ik_1(z + h + iq)}}{(z + h + iq)}dq \cong \frac{e^{ik_1R_1}}{R_1} + \frac{Z_g - 1}{Z_g + 1}\frac{e^{ik_1R_2}}{R_2}. \tag{31}$$

Equation (31) has the expected form of a downgoing spherical wave plus a reflection coefficient times an upgoing spherical wave. The result in Eq. (31) indicates that the Laplace transform method is not limited to nearly horizontal propagation.

Another limiting case of interest is $[R_2/(z + h)] \to \infty$. In this case, Eq. (29) can be approximated as

$$P_1(\bar{r}) \cong \frac{e^{ik_1R_1}}{R_1} + \frac{e^{ik_1R_2}}{R_2} - 2\frac{k_1}{Z_g}\frac{e^{ik_1R_2}}{R_2}\int_0^\infty e^{-(k_1/Z_g)q}dq$$
$$= \frac{e^{ik_1R_1}}{R_1} - \frac{e^{ik_1R_2}}{R_2}, \tag{32}$$

which is appropriate for $\theta \to 90°$.

As a final analytic limit, we consider grazing incidence and obtain from Eq. (29) the standard error function solution. For $R_2 \gg z + h$, the image integral in Eq. (29) can be approximated as

$$2\frac{k_1}{Z_g}\int_0^\infty e^{-(k_1/Z_g)q}\frac{e^{ik_1|\bar{r}+\hat{z}(h+iq)|}}{|\bar{r}+\hat{z}(h+iq)|}dq$$
$$\cong 2\frac{k_1}{Z_g}\frac{e^{ik_1R_2}}{R_2}e^{-d^2}\int_0^\infty \exp\left[-\left(\sqrt{\frac{ik_1}{2R_2}}q-id\right)^2\right]dq$$
$$=-\frac{e^{ik_1R_2}}{R_2}[1-R(\theta_0)]i\sqrt{\pi}de^{-d^2}\operatorname{erfc}(-id)\,, \quad (33)$$

where erfc is the complementary error function and θ_0 is defined through the relations

$$\sin(\theta_0)=\frac{\rho}{R_2}\,,\quad \cos(\theta_0)=\frac{z+h}{R_2}\,. \quad (34)$$

The numerical distance d and the reflection coefficient $R(\theta_0)$ are defined, respectively, as

$$d=\sqrt{\frac{ik_1R_2}{2}}\frac{Z_g\cos\theta_0+1}{Z_g}\,, \quad (35)$$

$$R(\theta_0)=\frac{Z_g\cos\theta_0-1}{Z_g\cos\theta_0+1}\,. \quad (36)$$

For the quantity $|\bar{r}+\hat{z}(h+iq)|$ in the exponent in Eq. (33), we use the approximation

$$|\bar{r}+\hat{z}(h+iq)|\equiv\sqrt{\rho^2+(z+h+iq)^2}$$
$$\cong R_2+i\cos\theta_0 q-\frac{1}{2R_2}q^2 \quad (37)$$

and in the denominator the approximation,

$$|\bar{r}-\hat{z}(h+iq)|\equiv\sqrt{\rho^2+(z+h+iq)^2}\cong R_2\,. \quad (38)$$

Substituting Eq. (33) into (29), gives

$$P_1(\bar{r})\cong\frac{e^{ik_1R_1}}{R_1}+\frac{e^{ik_1R_2}}{R_2}$$
$$\times\{1+[1-R(\theta_0)]i\sqrt{\pi}de^{-d^2}\operatorname{erfc}(-id)\}$$
$$=\frac{e^{ik_1R_1}}{R_1}+\frac{e^{ik_1R_2}}{R_2}\{R(\theta_0)+[1-R(\theta_0)]F(d)\}\,, \quad (39)$$

with

$$F(d)=1+i\sqrt{\pi}de^{-d^2}\operatorname{erfc}(-id)\,. \quad (40)$$

The result in Eq. (39) agrees with the error function solution of other authors.[2,3,6,9]

IV. NUMERICAL CALCULATION

In this section we discuss the details of numerically evaluating the integral in Eq. (29). As the integral stands, the upper limit on q is infinity. Hence we want to examine the integrand to see what upper limit is actually required for a useful result in typical calculations. We show a simple means for establishing a general upper limit that allows a straightforward numerical evaluation of the integral. To demonstrate the accuracy of the approach, we apply it to two different propagation problems.

In establishing a general upper integration limit, we take a conservative approach and assume the falloff of the integrand in Eq. (29) is controlled primarily by the factor $\exp(-k_1q/Z_g)$, which we shall call the "source strength factor." This assumption sometimes gives an upper limit that is greater than actually needed. However, since the integrand is so easily computed, a more sophisticated analysis does not seem worthwhile.

We write the source strength factor as

$$\exp(-k_1q/Z_g)=\exp(-\alpha q)\exp(i\beta q)\,, \quad (41)$$

where

$$\alpha=k_1R/(R^2+X^2) \quad (42)$$

and

$$\beta=k_1X/(R^2+X^2)\,. \quad (43)$$

Hence in terms of the real and imaginary parts of Z_g (R and X, respectively) we have the relation $\beta=(X/R)\alpha$.

Since the real exponential $\exp(-\alpha q)$ in the source strength factor dominates the image integral, we can estimate an upper limit for numerical integration, q^*_{upper}, by choosing $q^*_{\text{upper}}=\text{constant}/\alpha$. For our purposes it suffices to choose the constant to be 2π and write

$$q^*_{\text{upper}}=\frac{2\pi}{\alpha}=\frac{X^2+R^2}{R}\lambda\,, \quad (44)$$

where λ is the acoustic wavelength in air. (Note that in actual calculations a more conservative upper limit on the integration could be used. For example, one might use $q_{\text{upper}}=1.5q^*_{\text{upper}}$.)

With the value in Eq. (44) for q^*_{upper}, the real exponential decays to $\exp(-2\pi)\approx 0.002$ over the integration range. Over the same interval, the complex exponential $\exp(i\beta q)=\exp[i2\pi(X/R)(q/q^*_{\text{upper}})]$ undergoes X/R oscillations. For realistic ground impedances we often have $X/R\approx 1$, and in general we can expect X/R to be less than 10.[15,16] Hence no matter whether one chooses the constant to be 2π or some other value, having $X/R<10$ assures us that the source strength factor does not oscillate wildly. Thus for realistic ground surfaces we can expect the source strength factor $\exp(-k_1q/Z_g)$ to be bounded and well-behaved.

As a first application of the method we consider propagation over a locally reacting ground surface with source and receiver heights that are typical of experiments in outdoor sound propagation, 1.8 and 1.5 m, respectively. Figure 2 shows examples of the normalized image integral integrand as a function of q for a propagation range of 1500 m. In the figure the value of q^*_{upper} is indicated with an arrow on the q axis. The following values for frequency, impedance, and q^*_{upper} were used: (a) $f=100$ Hz, $Z_g=(13, 12.4)$, $q^*_{\text{upper}}=84.4$; (b) $f=200$ Hz, $Z_g=(8, 10)$, $q^*_{\text{upper}}=34.9$; (c) $f=500$ Hz, $Z_g=(7.2, 8.2)$, $q^*_{\text{upper}}=11.3$; (d) $f=1000$ Hz, $Z_g=(6, 4)$, $q^*_{\text{upper}}=3$. The values for q^*_{upper} were computed from Eq. (44), and the values used for Z_g are realistic impedances for grass-covered ground.[15,16] We have used impedance values with $X/R\approx 1$ so that $\exp(i\beta q)$ has a single oscillation. This choice makes it easy to see that the total integrand in Fig. 2 is practically zero when $q\approx q^*_{\text{upper}}$, regardless of the frequency.

For cases where the ratio X/R is considerably greater that unity, the factor $\exp(i\beta q)$ has many oscillations, but the total integrand still becomes negligibly small when

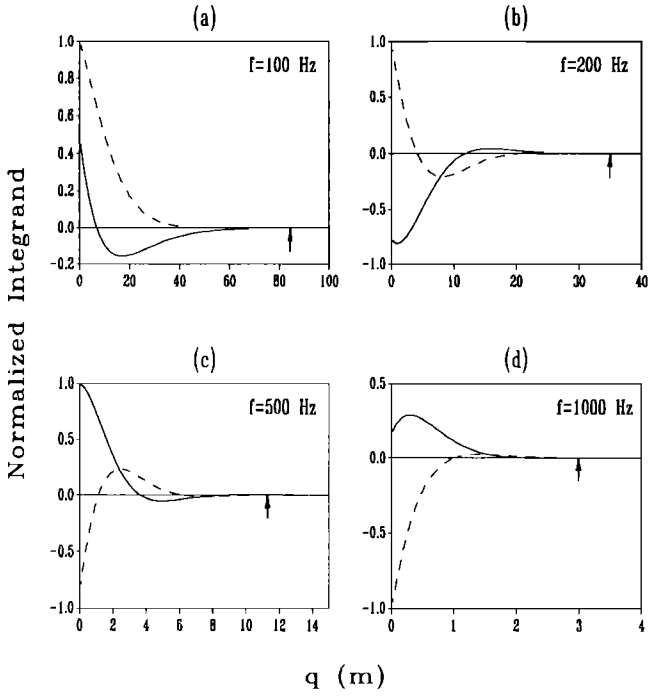

FIG. 2. Normalized integrands of the image integral at several frequencies as a function of q, the imaginary part of the image source position. The propagation range is 1500 m, and the source and receiver heights are 1.8 m and 1.5 m, respectively. The solid and dashed lines are, respectively, the real and imaginary parts of the integrand. The arrows indicate the estimated q values, q^*_{upper}, that would be used for the upper limit of integration. The numerical values for impedance and q^*_{upper} are given in the text.

$q \approx q^*_{\text{upper}}$. Hence, with enough integration points to track the additional oscillations, the integral can be easily computed by numerically integrating to $q \approx q^*_{\text{upper}}$ using a simple integration scheme such as the trapezoidal rule. Alternatively, one could use a specialized integration scheme, such as Filon integration,[17] which is designed specifically for oscillatory integrands. However, since the integrand can be evaluated very quickly, sophisticated integration schemes are probably only worthwhile in applications such as broadband propagation where extreme speed is valuable.

In the above example we considered a single range. To see the influence of the range on the convergence rate, we show in Fig. 3 the excess attenuation at 500 Hz as a function of range for different values of a variable integration limit, q_{upper}. [Note: We define excess attenuation as $-20\log_{10}(P_1 R_1)$, where P_1 is defined in Eq. (29), and R_1 is defined in Fig. 1. The excess attenuation defined here is transmission loss minus spherical spreading loss.] At 500 Hz, the value of the estimated upper limit, q^*_{upper}, is 11.3. When $q_{\text{upper}} \geqslant 13 = 1.15 q^*_{\text{upper}}$, the excess attenuation converges to a fixed value at any given range, as one would expect from the results shown in Fig. 2.

Finally we compare the convergent result in Fig. 3 to a parabolic equation (PE) calculation.[18,19] Figure 4 shows that the agreement is very good, as the two curves overlay almost perfectly. The agreement between the two completely different calculations gives us confidence that both are numerically accurate solutions to the given problem.

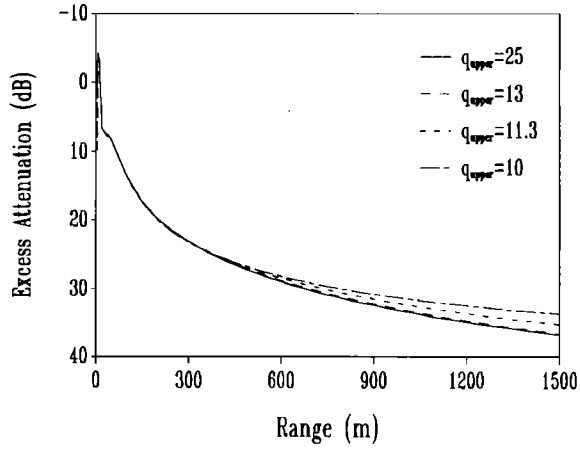

FIG. 3. Convergence test for the calculation in Fig. 2. The input parameters are the same as in Fig. 2, except for the upper integration limit, q_{upper}, which takes on the values shown in the figure.

In the above example, where the source and receiver were at typical measurements heights, the free-space Green's function, $\exp[i|\bar{r} + \hat{z}(h + iq)|]/|\bar{r} + \hat{z}(h + iq)|$, in the image integral in Eq. (29), was extremely well-behaved. Consequently the image integral was straightforward to compute numerically. With trapezoidal integration, for example, 10 to 20 points gave acceptable accuracy. In cases where the source and receiver are closer to the ground (within a small fraction of a wavelength), the free-space Green's function can cause the total integrand to be oscillatory so that more integration points are needed. As an extreme case we consider a second example in Fig. 5 where the frequency is again 500 Hz, but the source and receiver are both 0.01 m above the ground. The figure shows the normalized integrand versus q for a worst-case situation (range $= q^*_{\text{upper}} = 11.3$ m). Even though the integrand is oscillatory, it nevertheless is negligible when $q \approx q^*_{\text{upper}}$, so its integral is still

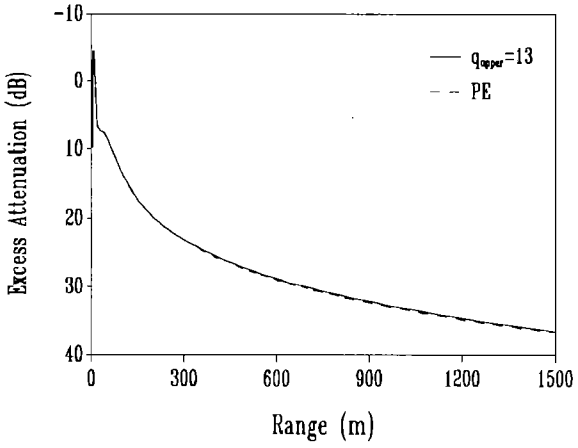

FIG. 4. Excess attenuation versus range for $f = 500$ Hz, $Z_g = (7.19, 8.2)$, and source and receiver heights of 1.8 and 1.5 m, respectively. The solid line is obtained from numerical integration of Eq. (29) with $q_{\text{upper}} = 13$ m as the upper integration limit. The dashed line is a parabolic equation calculation based on the method in Refs. 18 and 19.

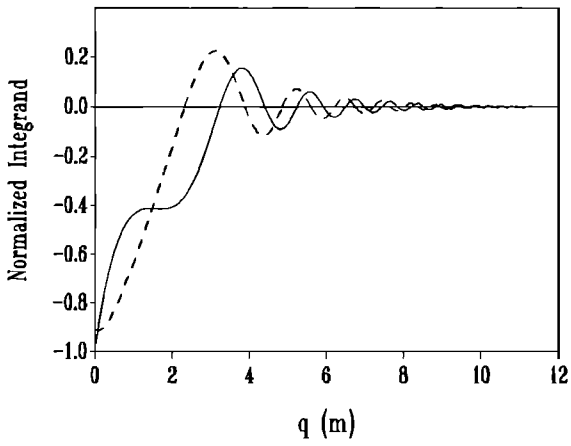

FIG. 5. Normalized integrand of the image integral as a function of q, the imaginary part of the image source position. The frequency is 500 Hz, and the ground impedance is (7.19, 8.2). The propagation range is 11.3 m, and the source and receiver are both at a height of 0.01 m. The solid and dashed lines are, respectively, the real and imaginary parts of the integrand.

easily computed. In Fig. 6 we compute the excess attenuation versus range using the same upper integration limit as before ($q_{\text{upper}} = 1.15 q^*_{\text{upper}}$) and again compare the image result to a PE calculation. Since there is a small difference (about 1 dB) between the PE calculation and the image result, we include the standard error function solution,[2,3,6,9] given in Eqs. (39) and (40), as an independent check. The error function solution is accurate for small grazing angles and, as expected, is in excellent agreement with the image result. Hence we can conclude that the image calculation and error function solution are both accurate and that the PE calculation is slightly in error. The small error in the PE calculation is a result of using a PE starting field that does not exactly satisfy the boundary condition at $z = 0$ for a source very near the ground. Figure 6 shows clearly the value of having an exact solution as a check for a general but approximate method such as the PE.

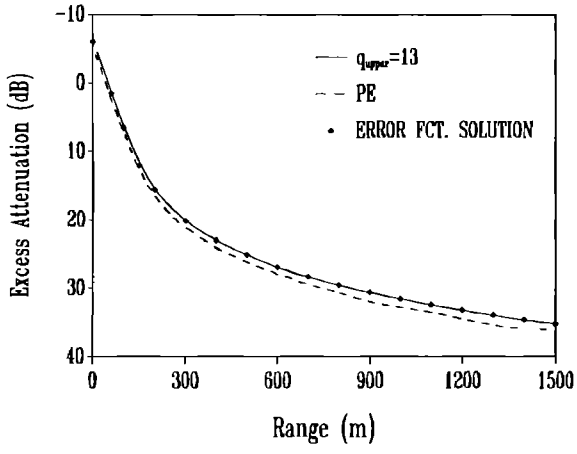

FIG. 6. Same as in Fig. 4 except the source and receiver are both at 0.01 m. The error function solution given in Eqs. (39) and (40) is included as an independent check. The agreement between the image calculation and the error function solution indicates that both results are accurate and that the PE calculation is slightly in error.

For the comparison shown in Fig. 6, 64 integration points were needed to obtain an accurate result. Even though a considerable number of points were required, the calculation was still very fast because the integrand can be computed rapidly. In addition, because a general upper limit on the integration was known, we could easily automate the calculation by having the computer program increase the number of integration points in the interval $[0, 1.15\, q^*_{\text{upper}}]$ until the desired level of accuracy was reached. Thus the method described here allows a numerical result of arbitrary accuracy to be computed with ease.

V. SUMMARY AND CONCLUSIONS

In this article we write the total acoustic field due to a point source above a complex impedance plane as the free-space field plus an image-source field. It is shown that the image is a line source that lies in a complex z space. The formulation is simple, concise, and intuitive. Unlike the Sommerfeld integral approach, which invariably results in a steepest descent approximation and later an error function integral, the exact image integral obtained here can be numerically integrated with ease. The accuracy of the solution can be checked by the convergence of the integral itself, which proves to be very fast. The method presented here appears to be a useful alternative to existing methods for computing sound propagation in a homogeneous atmosphere above a ground surface, especially for applications where an exact numerical result is needed.

ACKNOWLEDGMENTS

This work was supported by the NASA Langley Research Center. The authors would like to acknowledge several useful discussions with W. Pat Arnott.

[1] I. Rudnick, "The propagation of an acoustic wave along a boundary," J. Acoust. Soc. Am. **19**, 348–356 (1947).
[2] R. B. Lawhead and I. Rudnick, "Acoustic wave propagation along a constant normal impedance boundary," J. Acoust. Soc. Am. **23**, 546–549 (1951).
[3] U. Ingard, "On the reflection of a spherical sound wave from an infinite plane," J. Acoust. Soc. Am. **23**, 329–335 (1951).
[4] D. I. Paul, "Acoustical radiation from a point source in the presence of two media," J. Acoust. Soc. Am. **29**, 1102–1109 (1957).
[5] A. R. Wenzel, "Propagation of waves along an impedance boundary," J. Acoust. Soc. Am. **55**, 956–963 (1974).
[6] C. F. Chien and W. W. Soroka, "Sound propagation along an impedance plane," J. Sound Vib. **43**, 9–20 (1975).
[7] S. I. Thomasson, "Reflection of waves from a point source by an impedance boundary," J. Acoust. Soc. Am. **59**, 780–785 (1976).
[8] R. J. Donato, "Propagation of a spherical wave near a plane boundary with a complex impedance," J. Acoust. Soc. Am. **60**, 34–39 (1976).
[9] K. Attenborough, S. I. Hayek, and J. M. Lawther, "Propagation of sound above a porous half-space," J. Acoust. Soc. Am. **68**, 1493–1501 (1980).
[10] T. Kawai, T. Hidaka, and T. Nakajima, "Sound propagation above an impedance boundary," J. Sound Vib. **83**, 125–138 (1982).
[11] P. J. T. Filippi, "Extended source radiation and Laplace type integral representation: application to wave propagation above and within layered media," J. Sound Vib. **91**, 65–84 (1983).
[12] M. A. Nobile and S. I. Hayek, "Acoustic Propagation over an impedance plane," J. Acoust. Soc. Am. **78**, 1325–1336 (1985).

[13] I. V. Lindell and E. Alanen, "Exact image theory for the Sommerfeld half-space problem, part I: vertical magnetic dipole," IEEE Trans. Antennas Propagat. **AP-32** (2), 126–133 (1984).
[14] I. V. Lindell and E. Alanen, "Exact image theory for the Sommerfeld half-space problem, part II: vertical electric dipole," IEEE Trans. Antennas Propagat. **AP-32** (8), 126–133 (1984).
[15] G. A. Daigle and M. R. Stinson, "Impedance of grass-covered ground at low frequencies measured using a phase difference technique," J. Acoust. Soc. Am. **81**, 62–68 (1987).
[16] T. F. W. Embleton and G. A. Daigle, "Atmospheric Propagation," in *Aeroacoustics of Flight Vehicles: Theory and Practice*, edited by H. H. Hubbard (NASA Langley Research Center, Hampton, VA, 1991), [NASA Ref. Pub. 1258, Vol. 2; also WRDC Tech. Rep. 90-3052 (1991), Chap. 12].
[17] *Handbook of Mathematical Functions with Formulas, Graphs, and Mathematical Tables*, edited by M. Abramowitz and I. A. Stegun (U.S. Government Printing Office, Washington, DC, 1967), NBS Appl. Math. Ser. 55, p. 890.
[18] K. E. Gilbert and M. J. White, "Application of the parabolic equation to sound propagation in a refracting atmosphere," J. Acoust. Soc. Am. **85**, 630–637 (1989).
[19] K. E. Gilbert, R. Raspet and X. Di, "Calculation of turbulence effects in an upward-refracting atmosphere," J. Acoust. Soc. Am. **87**, 2428–2437 (1990).